

XMM OBSERVATIONS OF ULTRALUMINOUS X-RAY SOURCES IN NEARBY GALAXIES

HUA FENG AND PHILIP KAARET

Department of Physics and Astronomy, The University of Iowa, Iowa City, IA 52242; hua-feng@uiowa.edu
Draft version February 7, 2020

ABSTRACT

We examined X-ray spectral and timing properties of ultraluminous X-ray sources (ULXs) in nearby galaxies in *XMM-Newton* archival data. There appear to be three distinct classes of spectra. One class shows emission from hot, diffuse plasma. This thermal emission is similar to that seen from recent supernovae; the temperatures are in the range 0.6–0.8 keV and the luminosities are the lowest in our sample, near 10^{39} erg/s. Three sources have spectra which are strongly curved at high energies and have the highest temperatures in our sample, 1.0–1.4 keV. These spectra are well fitted with a power-law plus multicolor disk blackbody model with the power-law dominant at low energies or a Comptonization model. The remainder of the sources are best fitted with a power-law plus multicolor disk blackbody model, as is commonly used to describe the spectra of accreting black holes. These sources have the lowest thermal component temperatures, 0.1–0.4 keV, and extend to the highest luminosities, above 10^{40} erg/s. The temperature of the thermal component is in three distinct ranges for the three source classes. This diversity of spectral shapes and the fact that the sources lie in three distinct temperature ranges suggests that the ULXs are a diverse population. Two ULXs which show state transitions stay within a single class over the course of the transition. However, we cannot conclude with certainty that the classes represent distinct types of objects rather than spectral states of a single population of objects. More monitoring observations of ULXs with *XMM-Newton* are required. We also searched for timing noise from the sources and report detection of noise above the Poisson level from five sources. In three of the sources, the power density spectrum increases with decreasing frequency as a power-law down to the lowest frequencies observed, below 10^{-4} Hz.

Subject headings: black hole physics — accretion, accretion disks — X-rays: binaries — X-rays: galaxies

1. INTRODUCTION

Non-nuclear ultraluminous X-ray sources (ULXs) in external galaxies have been known since the *Einstein* era (Fabbiano 1989) with apparent isotropic luminosities above the Eddington limit of a $10M_{\odot}$ black hole ($L \approx 2 \times 10^{39}$ erg/s) (for reviews see Fabbiano & White 2003; Miller & Colbert 2004). From the surveys of nearby galaxies undertaken with the *ROSAT* HRI (Colbert & Ptak 2002) and the *Chandra* ACIS (Swartz et al. 2004), more than one hundred sources with luminosity greater than 10^{39} erg/s have been located in nearby galaxies.

The nature of ULXs is still unclear. The major dispute arises from our observational ignorance of the angular distribution of the source emission. If X-rays are emitted isotropically, then the high luminosity indicates that the ULXs might harbor intermediate mass black holes (IMBHs) with the mass in the order of $100M_{\odot}$ or even higher (Colbert & Mushotzky 1999; Makishima et al. 2000; Ptak & Griffiths 1999; Kaaret et al. 2001). If the emission is beamed, then the ULXs could be stellar mass black holes (King et al. 2001; K rding et al. 2002).

Evidence that the luminosities are truly high for some ULXs has been found from their associations with optical nebula which show indications of X-ray ionization (Pakull & Mirioni 2003). The photoionizing flux required to power the nebula surrounding one ULX requires a luminosity greater than 4×10^{39} erg/s (Kaaret et al. 2004). Optical nebulae associated with some ULXs also show shock emission indicative of unusually powerful explosions (Pakull & Mirioni 2003).

X-ray spectral analysis has revealed thermal components in the spectra of several ULXs with temperatures of 0.1–0.3 keV (Colbert & Mushotzky 1999; Kaaret et al. 2003; Miller et al. 2003), which are lower than that in stellar mass black holes in high states, suggesting accretion onto a black hole with higher mass (Makishima et al. 2000). Also, a few ULXs exhibit breaks in their timing power spectra at relatively low frequencies which have been interpreted as evidence for high black hole masses (Cropper et al. 2004; Soria et al. 2004). However, such interpretations are ambiguous due to our lack of understanding of timing power spectra and the fact that some stellar-mass black holes occasionally exhibit breaks at similar frequencies (McClintock & Remillard 2004).

XMM is more powerful for spectral and timing analysis than previous X-ray telescopes owing to its large effective area. The goal of this paper is to use *XMM* archival data to study the spectral and timing behaviors of ULXs in nearby galaxies. In § 2 we describe the details of data reduction. We present the spectral analysis and details for some selected ULXs in § 3 and timing analysis and results in § 4. Finally, we interpret our results in § 5.

2. DATA REDUCTION

We derive our source sample from previously reported ULX detections. Specifically, we used the *Chandra* catalog of Swartz et al. (2004), the *ROSAT* catalog of Colbert & Ptak (2002), and the catalog of Liu & Mirabel (2005). We included only sources located in nearby galaxies with distances less than 11 Mpc. We selected sources with enough counts in *XMM* exposures for good

spectral and timing analysis. We eliminated sources crowded near other point sources that can not be resolved by *XMM*, e.g. the ULXs in M82. Starting from these three catalogs and applying the criteria above, which are solely intended to enable us to perform reliable spectral and timing analysis, we produced a final sample of 28 sources, see Table 1. Hereafter we refer to sources by their number in Table 1 since not every ULXs has a common name. Our sample is not meant to constitute an unbiased survey of nearby galaxies for ULXs. Rather, it is intended to provide a sample with which we can examine the spectral and timing properties of sources previously reported as ULXs in the literature.

All data were processed using *SAS* 6.1.0 with the most recent calibration files as of March 2005. We extracted single and double events (*PATTERN* ≤ 4) for pn data with the addition of triple events (*PATTERN* ≤ 12) for MOS data. For spectral analysis, we required *FLAG* = 0 and screened for good time intervals without background flares. For timing analysis, we required *FLAG* equal to *#XMMEA_EM* for MOS and *#XMMEA_EP* for pn, and selected a continuous good time interval without background flare contamination or data gaps. We found that gaps in the *XMM-Newton* data stream often cause spurious timing signals in the frequency region $10^{-4} \sim 10^{-2}$ Hz. Therefore it is better to avoid gaps than attempt to fill them, e.g. with an average count rate.

Source counts are generally extracted from a $32''$ -radius circle, following the recommendation in the data analysis threads on the *XMM SAS* web page at <http://xmm.vilspa.esa.es/sas/documentation/threads/>. For some very bright isolated sources, we used a $40''$ -radius circle (this results in an increase in luminosity by a few percents but no difference in spectral parameters within errors). For sources in crowded regions or with a strong diffuse background, we used a source region with a $16''$ -radius circle. To attain the best statistics, we combine the data from the pn and the two MOS detectors unless some CCD detectors are turned off, the source rides on the gap between two CCD chips in one of the detectors, or the source is located at the edge of a CCD chip. The energy spectra are extracted from individual MOS and pn detectors and then grouped for fitting. The light curves are obtained from the merged events files.

3. SPECTRAL ANALYSIS AND RESULTS

The energy spectra are fitted with *XSPEC* 11.3.1. First, we fit all 28 sources with a single power-law spectrum and, separately, with a single multicolor disk (MCD) (Mitsuda et al. 1984; Makishima et al. 1986, *diskbb* in *XSPEC*) spectrum. Both spectral models, and all others considered here, also include interstellar absorption. The absorption column density is treated as a free parameter with a lower bound set to the column density along the line of sight within the Milky Way (Dickey & Lockman 1990) for all models in this paper. Then we tried adding a MCD component to each power-law model. We accept the MCD component if its addition improves the fit by at least 4σ significance as calculated using the F-test for an additional component. The spectral parameters from all the fits, the unabsorbed 0.3–10 keV luminosities calculated assuming isotropic emission, and χ^2/dof for each fit are listed in Table 2. We

include only those fits with $\chi^2/\text{dof} \leq 1.4$. We find 13 sources with a significant MCD component in addition to the the power-law component. In half of these sources, the power-law is dominant at high energies and the MCD disk temperature is in the range 0.1–0.4 keV.

Source 1 is better fitted with a single MCD model than with a single power-law model. The F-test shows that the MCD model is preferred at a significant level of 0.05. For sources 2, 11, 13–16 and 19–21, the F-test shows no preference for a single MCD or a single power-law. For sources 9, 10, 18, 24, and 27, the χ^2/dof for the single MCD model is greater than 1.4, therefore that model is rejected, and no significant improvement was obtained with the MCD plus powerlaw model. For these sources, only the powerlaw fit is reported.

The spectra of sources 12, 22 and 26 show significant residuals when fitted with a MCD plus power-law model and have $\chi^2/\text{dof} > 1.7$. Therefore, we searched for another spectral model which would give a better fit. All three spectra show a bump around 0.5–1.0 keV, which is a region where hot diffuse gas produced significant

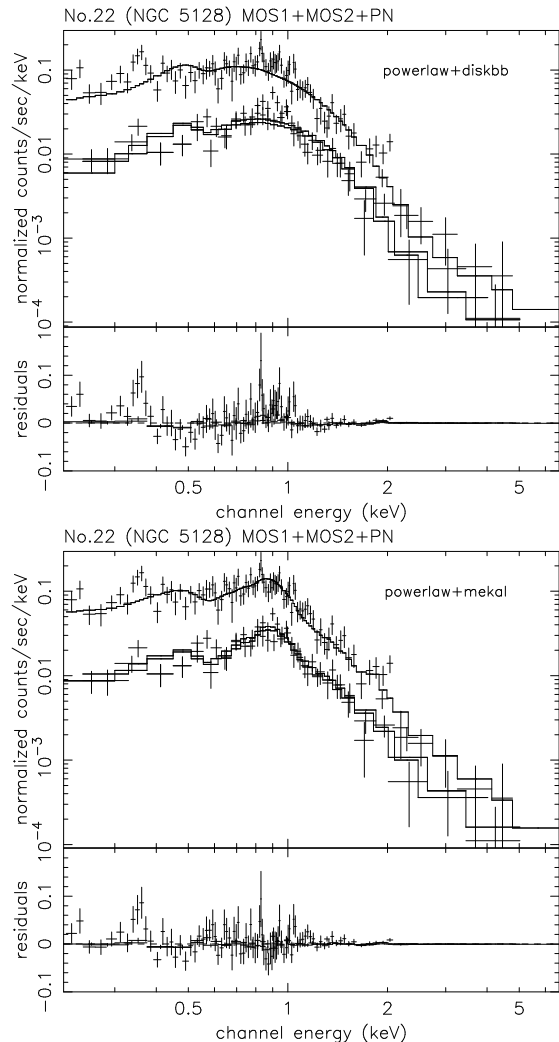


FIG. 1.— Energy spectra of source 22 fitted with an MCD model plus power-law model (top) or with a mekal plus power-law model (bottom). The mekal model is a significantly better fit to the spectrum because it adequately models the bump around 0.5–1.0 keV.

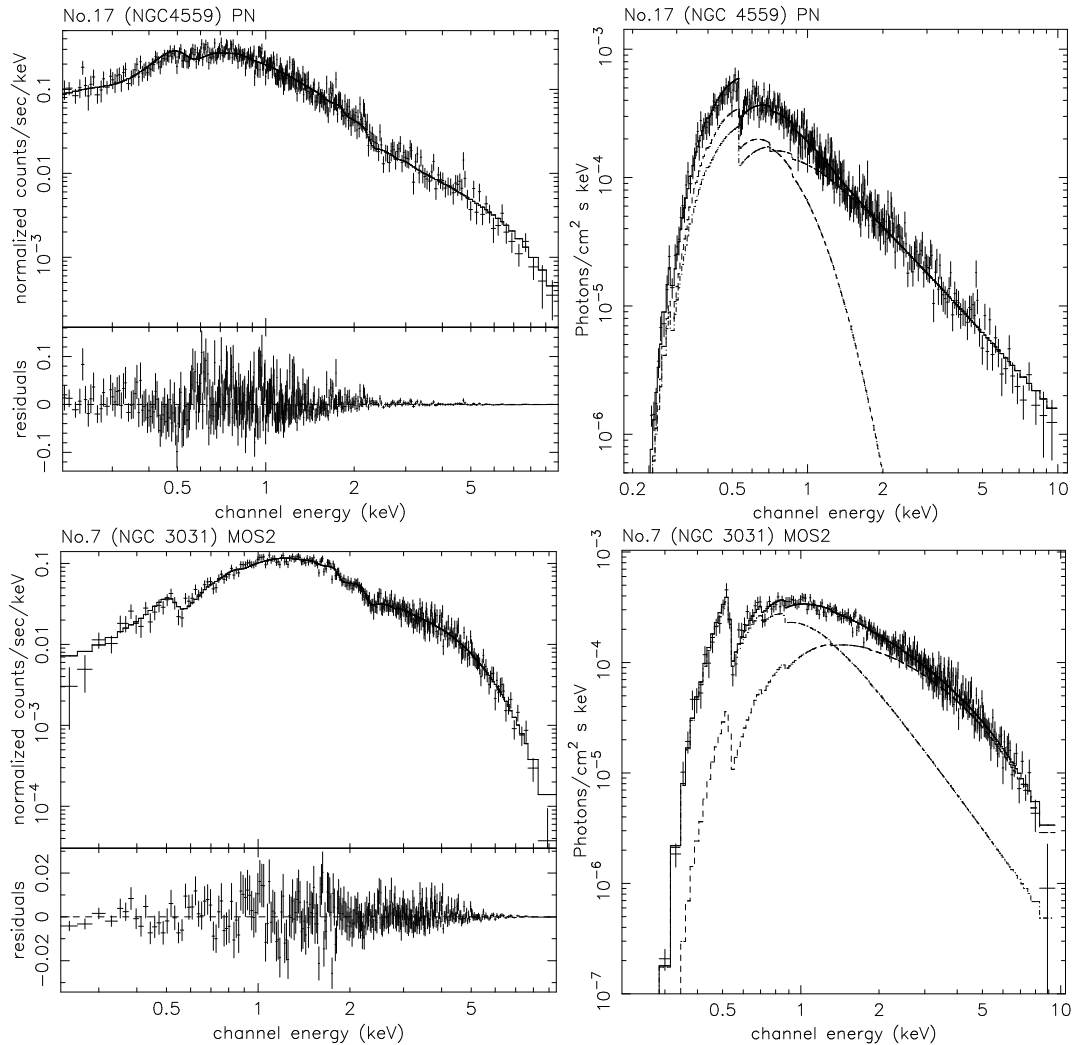


FIG. 2.— Energy spectra of sources 17 and 7. The spectrum of source 17 (top left) consists of a 0.17 keV MCD and a power-law (top right). The spectrum of source 7 is curved at high energy (bottom left) which could be fitted either by a combination of a 1.51 keV MCD and a power-law (bottom right) or by a single Comptonization model (not shown).

line emission. We found that the sum of a hot diffuse gas model (Mewe et al. 1995, mekal in *XSPEC*) plus a power-law produced a much better fit than the MCD plus power-law model for all three sources. A comparison of the two models for source 22 is shown in Fig. 1.

For sources 3, 6, and 7, the MCD component is dominant at high energies. We fitted the spectra for these three sources with a single MCD model and with a single Comptonization model (Sunyaev & Titarchuk 1980, *compst* in *XSPEC*). The single MCD model fits are not poor, with $\chi^2_\nu = 1.2 \sim 1.3$, but are rejected compared to the MCD plus power-law model or the Comptonization model. The Comptonization model fits, with large optical depth $\tau \approx 20$, are as good or better than the power-law plus MCD model fits. These three sources shown significant curvature in the high energy parts of their spectra, which is quite distinct from the power-law followed by most of the other sources at high energies. Fig. 2 shows the spectrum of source 17, which is best fitted with an MCD plus power-law with the power-law dominant at high energies and which is typical of the sources with low disk temperatures, $kT = 0.1 - 0.4$ keV.

In contrast, the spectrum of source 7 is the strongly curved at high energies, as shown fitted with an MCD plus power-law model in which the MCD component is dominant at high energies or a Comptonization model. The spectra of sources 3 and 6 have the same shape as source 7.

In Fig. 3, we plot source luminosity L versus photon index Γ for sources with and without a significant thermal component. For sources without a thermal component there is no apparent correlation between luminosity and photon index. For sources with a thermal component, there appears to be an absence of sources with hard spectra at low luminosities, i.e. in the bottom left corner of the bottom panel of Fig. 3.

The relation between the photon index Γ of the power-law component and the temperature kT of the thermal component is shown in Fig. 4 for all sources where addition of the thermal component significantly improves the fit. Considering all sources together, high temperatures appear to be correlated with soft photon indices. However, this correlation appears to be a by-product of the juxtaposition of different spectral shapes. In particular,

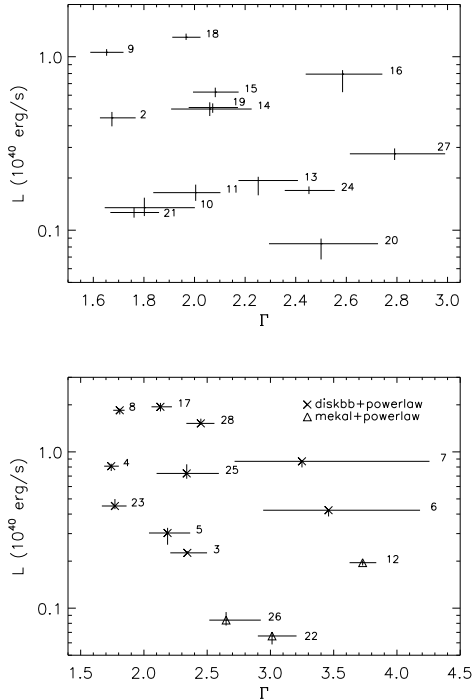


FIG. 3.— Luminosity vs. photon index of ULXs. Top: ULXs with a single power-law spectrum; Bottom: ULXs with a prominent MCD component plus the power-law spectrum. The label indicates the source index number in Table 1.

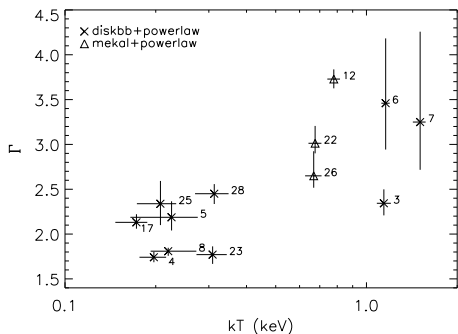


FIG. 4.— Photon index vs. temperature of ULXs with a prominent thermal component plus the power-law spectrum. The label indicates the source index number in Table 1.

sources 3, 6 and 7 which have the highest temperatures are well fitted by a single Comptonization model or a power-law plus MCD model with the power-law is dominant at low energies and the thermal component at high energies, in contrast to the other sources. The intermediate temperature sources, 12, 22, and 26, are exactly those better fitted by a mekal model than a MCD model. Considering only the sources for which the power-law plus MCD is the best fit and the power-law dominates at high energies, there is no correlation apparent between Γ and kT .

Fig. 5 shows the relationship between the temperature kT of the thermal component and the X-ray luminosity L , for all sources where addition of the thermal component significantly improves the fit. Again, the sources

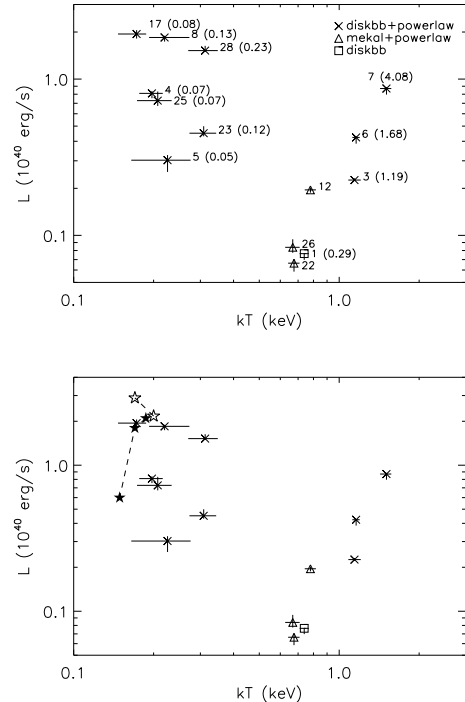


FIG. 5.— Luminosity vs. temperature of ULXs with a significant thermal component in their spectra. The label indicates the source index number in Table 1 and the fractional Eddington luminosity in the brackets which is derived from the MCD model (for details, see the text). In the bottom panel, two ULXs which have been observed with *XMM-Newton* to undergo state transitions are added. The filled stars represent Holmberg II X-1 (Dewangan et al. 2004) and the white stars represent Holmberg IX X-1 (Wang et al. 2004). The dashed lines connect individual sources observed in different states.

segregate according to the best fitting spectral model. Sources 3, 6 and 7 have the highest temperatures and cover a wide luminosity range extending up to 10^{40} erg/s. The sources with mekal components or a single MCD are at intermediate temperatures and relatively low luminosities. The sources for which the power-law plus MCD is the best fit tend to have low temperatures and relatively high luminosities. There is no correlation apparent between L and kT if we consider only the latter sources.

We can, crudely, estimate the ratio of the observed luminosity to the Eddington luminosity using the fitted temperature and X-ray luminosity. By adopting the canonical values of the color correction and temperature profile correction in Makishima et al. (2000), the disk blackbody temperature scales with black hole mass as

$$kT = 1.2\beta^{-\frac{1}{2}}\eta^{\frac{1}{4}} \left(\frac{M}{10M_{\odot}} \right)^{-\frac{1}{4}} \text{ keV}, \quad (1)$$

where β is determined by the black hole spin, $\beta = 1$ for a Schwarzschild black hole and $\beta = 1/6$ for a maximally rotating Kerr black hole, and η is the bolometric luminosity normalized to the Eddington luminosity as $\eta = L_{\text{bol}}/L_{\text{Edd}}$. We take $L_{\text{Edd}} = (1.3 \times 10^{38} \text{ erg/s}) (M/M_{\odot})$ and approximate $L_{\text{bol}} = L_{\text{X}}$. Solving for η , we find the fractional Eddington luminosity

$$\eta = \beta \left(\frac{kT}{1.2 \text{ keV}} \right)^2 \left(\frac{L_X}{1.3 \times 10^{39} \text{ erg/s}} \right)^{1/2}. \quad (2)$$

We derive a fractional Eddington luminosity (shown in Fig. 5 in the brackets) from Eq. 2 with $\beta = 1$. There are three sources which appear to be above the Eddington limit, with L/L_{Edd} of 1.2, 1.7 and 4.1 respectively for sources 3, 6, and 7. If the black holes are rapidly rotating, as suggested by Makishima et al. (2000), then the sources fall below Eddington luminosity with source 7 still near the Eddington luminosity.

4. TIMING ANALYSIS AND RESULTS

After examining the power spectral density (PSD) of every source in our sample, we find three sources (No. 4, 23, & 25) with detectable noise power in the frequency range 0.001–0.1 Hz. The lower frequency bound is chosen based on the shortest good time interval of any observation used in this analysis in order to allow a uniform frequency range for all sources. The PSD in the other sources is consistent with Poisson fluctuations, and we can only place an upper limit on the noise power (see Fig. 6). There is no obvious correlation between the rms variability and the luminosity among those three sources with detectable noise power. The rms upper limits appear correlated with source luminosity because the sensitivity of the upper limit depends on the total number of counts recorded.

We are able to detect timing noise in several frequency bands for three sources, No. 7, 22, & 25. Light curves and PSDs for these three sources are presented in Fig. 7. All PSDs are normalized to rms (van de Klis 1988) and binned in logarithmic scale with points above the Poisson level plotted with error bars and points below the Poisson level plotted as an upper limit. We have checked the PSD from background regions for these observations to ensure that the timing noise is not produced by variations in the background. The noise power for sources 7 and 22 lies below 0.001 Hz. They do not have detectable noise power in 0.001–0.1 Hz band used above.

We note that the timing features reported by Cropper et al. (2004), including PSDs with a break power-law in source 17 (NGC 4559 X7) and a single power-law in source 18 (NGC 4559 X10), are not repeated in our results. We examined the same *XMM* observation and found multiple background flares distributed across the whole exposure. If we only extract light curves at clean intervals, even including several small flares and with a duration up to 80% of the whole exposure, no timing noise is present above the Poisson level. If we use the whole exposure including the background flares, we can reproduce the PSD reported by Cropper et al. (2004). We conclude that the features in the power spectra reported by Cropper et al. (2004) are caused by background flares.

No. 7 (NGC 3031) We calculated the PSF from a 40.6 ks good time interval without timing gaps or background flares for both the MOS2 and the pn CCDs in the first half of the observation. The second half of the observation contains strong background flares and was discarded. The PSD is calculated in the energy range 2–10 keV with a 4096-point FFT. This energy band was selected because the timing noise is strongest in this

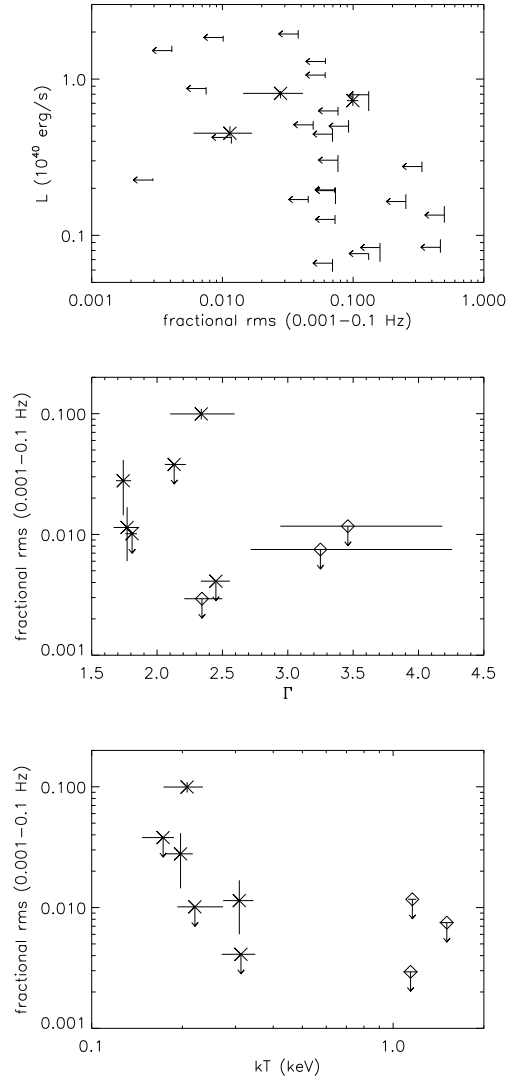


FIG. 6.— The relationship between the fractional rms integrated in the frequency region 0.001–0.1 Hz and the X-ray luminosity (top), power-law photon index (middle) and the thermal temperature (bottom). The luminosity is taken from the best-fitted spectrum. Three sources have detectable timing noise; these sources are best fitted with a MCD plus power-law spectrum. The sources for which timing noise above the Poisson level is not detected are shown as 2σ upper limits. In the middle and bottom panels, only sources which are well fitted with a MCD plus power-law model are plotted. Sources without detected noise are plotted only if the upper limit on the rms is less than 0.05. The diamonds indicate sources which were well fitted with a Comptonization model or a high temperature MCD plus power-law model.

band. For sources 22 and 25, we also present the PSD for the energy which maximizes the timing noise. The time resolution of the light curve is set to the interval duration divided by the number of FFT points (as for all these three sources). Power at frequencies below ~ 0.1 mHz increases at lower frequencies with power-law slope $\alpha = -1.8 \pm 0.3$. The PSD below 2 keV only has the lowest frequency point above the Poisson level.

No. 22 (NGC 5128) We select a 11.4 ks good time interval without gaps or background contamination for three MOS and pn CCDs. The PSD is calculated in the energy range 0.7–10 keV with a 1024-point FFT. We

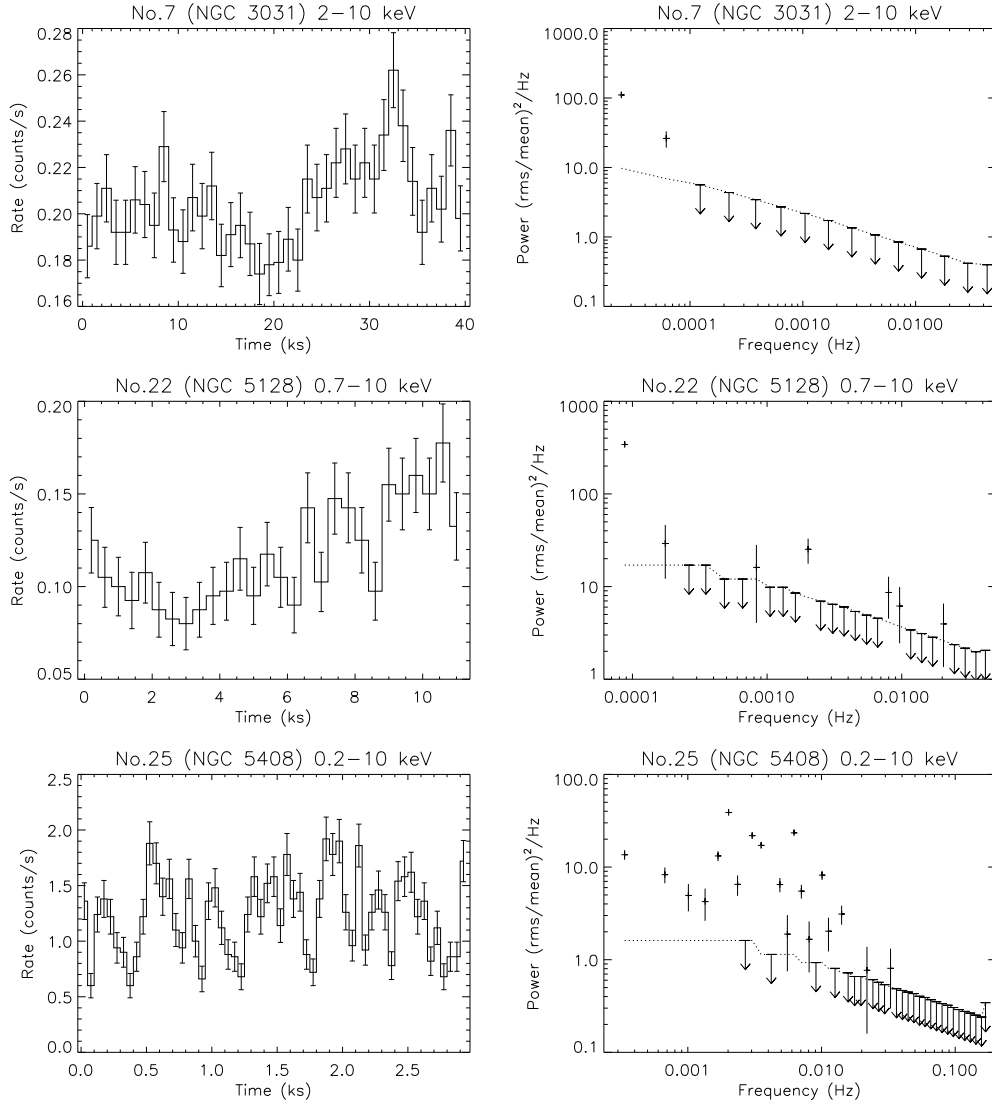


FIG. 7.— Light curves and power spectra of three ULXs.

also examined a power spectrum for events with energies below 0.7 keV, but there is no detectable power. The power spectrum below 0.2 mHz has a power-law slope $\alpha = -1.56 \pm 0.14$. There is also some power at frequencies around 2 mHz, but our sensitivity is inadequate to make unambiguous statements about this.

No. 25 (NGC 5408) The observation contains strong background flares in the second half and a 2.96 ks good time interval in the first half, which is used for calculation of the PSD. Soria et al. (2004) report a power spectrum for this observation with a power-law at high frequency breaking to a flat continuum ($\alpha = 0$) below a cutoff frequency of 2.5 mHz. Such a PSD is often found in Galactic black hole binaries and AGNs and the break frequency scales with mass, although the break frequency in individual sources varies by factors of at least 10. We re-examine the PSD in the 0.2–10 keV band with a 1024-point FFT. At frequencies below 0.001 Hz the power spectrum has a power-law slope $\alpha = -0.8 \pm 0.2$. Above this frequency, there appears to be power distributed ir-

regularly across a range associated with the flaring time scale reported by Soria et al. (2004). Our power spectrum does not suggest a break to a flat continuum with $\alpha = 0$ at low frequency. We are able to reproduce the spectrum reported by Soria et al. (2004) if we use much broader frequency bins.

5. DISCUSSION

We have found a diversity of spectra in our sample of ULXs. Considering only those sources for which the statistics justify the use of models more complex than a simple power-law, half the sources are best fitted with a MCD plus power-law model with the power-law dominant at high energies. This model is commonly used in fitting the spectra of accreting black holes. These sources have the lowest thermal component temperatures, 0.1–0.4 keV, and extend to the highest luminosities, above 10^{40} erg/s. Three sources have spectra which are strongly curved at high energies. These sources are best fitted with a MCD plus power-law model with the MCD component dominant at high energies and a steep

power-law at low energies or a Comptonization model. These sources have the highest temperatures in our sample, 1.0–1.4 keV. Three sources show evidence of diffuse hot plasma and are best fitted with a mekal model plus a power-law. The temperatures of these three sources are in the range 0.6–0.8 keV and the luminosities are the lowest in our sample, near 10^{39} erg/s. Finally, there is a single source best fitted with an MCD model alone. This source is likely a stellar-mass black hole in a high state. Within each class, the spectral parameters, particularly the emission temperature of the thermal component, appear to be rather similar. Between classes, the temperature of the thermal component varies significantly. This diversity of spectral properties and the fact that the sources appear to lie in three distinct classes, see Fig. 5, suggests that the ULXs are, in fact, a diverse population.

The three apparently distinct classes of ULXs may merely represent three states of ULXs and not a true diversity of physical objects. To examine if this is the case, we searched the literature for state transitions of ULXs in which the temperature of the thermal component has been measured. We found four such cases: Holmberg II X-1 (Dewangan et al. 2004), Holmberg IX X-1 La Parola et al. (2001); Wang et al. (2004), and two ULXs in IC 342 (Kubota et al. 2001). For Holmberg II and Holmberg IX X-1, multiple observations with *XMM-Newton* are available. We plot the spectral states of these sources, connected by dashed lines, in a bottom panel of Fig. 5. As can be seen from inspection of the figure, the ULXs which undergo state transitions remain within the same group in the luminosity vs temperature diagram. The state transitions do not move the sources between the groups. Both sources remain in the low kT throughout the state transitions. For the state transitions of the two ULXs in IC 342 reported by Kubota et al. (2001), both sources remain in the high kT group throughout the transitions. These sources are not plotted in Fig. 5 because we prefer to plot only spectra from *XMM-Newton* observations.

We note that La Parola et al. (2001) reported the state transition of M81 X-9 = Ho IX X-1 (source 8) with a high state observed by *ASCA* fitting by a single MCD model with a high temperature $kT = 1.24$ keV and a low state fitted by a power-law plus MCD model with $kT \sim 0.3$ keV. If correct, this would represent a transition between the low kT and high kT groups. However, Wang et al. (2004) reported two observations using *XMM-Newton* of Ho IX X-1 (one is the same as used in this paper). The luminosity during the *XMM-Newton* observations is a factor of 2 higher than in the *ASCA* observation and clearly represents the high state of the source. Wang et al. (2004) concluded a single MCD model, as used by La Parola et al. (2001) to fit the *ASCA* data, is strongly ruled out by the high quality *XMM-Newton* data. Instead, the spectra are better described by a cool disk plus power-law model. Their results are consistent with our own which rule out application of a single MCD model to the high state of Ho IX X-1. Therefore, we conclude that Ho IX X-1 remains in the low kT in its high and low states.

Those ULXs which undergo state transitions remain in the same class throughout the transition, suggesting that the definition of the different classes is robust. We

note that, on average, the low temperature ULXs are more luminous than the high temperature ones. Therefore, if the different classes represent different states of a single underlying population, then the lower luminosity states would be associated with higher temperatures, which is the reverse of the normal situation for black hole X-ray binaries. However, additional *XMM-Newton* observations of the sources in our sample would be of great interest to test if these source classes truly represent distinct classes of objects.

5.1. MCD plus power-law sources

Here, we consider the properties of the class of sources which are best fitted with MCD plus power-law model with the power-law dominant at high energies. In this class, there is an absence of sources with hard spectra at luminosities near 10^{39} erg/s. This is not the case for sources which lack a detectable thermal component. When a black hole is in its low/hard state, the disk temperature is low (McClintock & Remillard 2004). If these ULXs are intermediate mass black holes (IMBHs), then their temperature in low/hard states would shift out of the detection threshold of *XMM*. This would naturally produce an absence of sources with hard spectra at (relatively) low luminosities. This scenario would imply that the sources with single power-law spectra with hard spectra ($\Gamma \lesssim 2$) and luminosities near 10^{39} erg/s may be IMBHs in the low/hard state.

For accreting black holes in the high state, higher black hole masses should lead to cooler disk temperatures (Makishima et al. 2000). The low temperatures of some ULXs have been suggested to be evidence that they contain IMBHs (Colbert & Mushotzky 1999; Kaaret et al. 2003; Miller et al. 2003). In Fig. 5, the sources which are best fitted with a MCD plus power-law model with the power-law dominant at high energies concentrate at low temperatures, $kT < 0.4$ keV. Miller et al. (2004) have suggested that the clustering of ULXs in a narrow range in temperature is evidence that those ULXs are IMBHs with masses lying in a narrow range. However, current X-ray instrument lack the sensitivity to detect thermal components with temperatures much below 0.1 keV. Hence, the lower boundary of the range is observational. The thermal emission from higher mass black holes would simply not be detected.

In stellar mass black holes, different spectral states are associated with different levels of variability. The total noise power integrated in the 0.1–10 Hz band has an rms $\lesssim 0.06$ for high states and an rms of 0.1 to 0.3 for low states (McClintock & Remillard 2004). Because these relatively high frequencies are not accessible for ULXs given the sensitivity of *XMM-Newton*, we use the 0.001–0.1 Hz band to calculate the rms noise power. The relations between the rms noise level and the luminosity, thermal component temperature, and power-law photon index are shown in Fig. 6. For those three sources with detected rms, the noise does not appear correlated with luminosity. Also, the noise level does not appear correlated with photon index. Indeed, the one source which has a high noise level, as associated with the hard state of stellar-mass X-ray binaries, has a relatively soft photon index.

The X-ray variability of Galactic X-ray binaries at low frequencies has been examined by Gilfanov & Arefiev

(2005). In the frequency region from 10^{-4} to 0.1 Hz, the PSD of X-ray binaries is found to follow a power-law with an exponent α in the range -1.2 to -1.5 . The PSDs for source 7, 22 and 25 at low frequencies follow power-law forms with exponents α of -1.8 ± 0.3 , -1.56 ± 0.14 , and 0.8 ± 0.2 , respectively. These are similar to the PSDs of Galactic X-ray binaries at low frequencies. This may suggest that the PSDs reflect viscous variabilities from the accretion disks of the ULXs.

5.2. *Mekal sources*

The sources 12, 22 and 26 are not adequately fitted with a MCD plus power-law model. Their spectra present a prominent bump around 0.5–1.0 keV and their spectra are adequately fitted with the sum of a mekal thermal plasma model plus a power-law. The presence of a mekal component suggests that part of the X-ray emission from these sources arises from a hot, diffuse thermal plasem. The fractions of the total luminosity in the mekal component are 9.3%, 32.2% and 31.7% for source 12, 22 and 26, respectively.

We can place an upper bound on the physical size of these sources from that fact that all three sources appear unresolved with *Chandra*: Obs ID 402 for source 12, Kraft et al. (2001) for source 22, and Swartz et al. (2004) for source 26. Therefore their angular size must be less than $0''.5$. With this bound on the physical size and the mekal fit parameters temperature kT and normalization K , we can then derive a lower limit on the electron density $n \geq \sqrt{4\pi D^2 K / (10^{14} V)}$ (cm^{-3}), an upper limit on the total energy of $E \leq 2 \times \frac{3}{2} kT n V$ (erg), and an upper limit on the cooling time of $t \leq 1.05 \times 10^7 \sqrt{kT} / n$ (yr), where D is the distance to the host galaxy in cm, V is upper limit of the plasma volume $V \leq \frac{4}{3} \pi r^3$ in cm^3 , kT is the plasma temperature in keV, and the value and units of K are taken from *XSPEC*.

No. 12 (NGC 4395) The source is also known as NGC 4395 X-2 (Lira et al. 2000) located in the dwarf galaxy NGC 4395. In the *XMM* observation on 2003-Nov-30, the source is located near the gap in pn CCDs, leading to a small difference in flux between pn and MOS CCDs. Therefore we only take the two MOS CCDs for spectral analysis for this source. The spectral fitting gives $kT = 0.78 \pm 0.04$ keV and $K = 4.5 \pm 0.5 \times 10^{-5}$, from which we derive $n \geq 9.3 \text{ cm}^{-3}$, $E \leq 2.8 \times 10^{51}$ erg and $t \leq 1.0 \times 10^6$ yr.

No. 22 (NGC 5128) The source is located near the edge of southwest radio lobe in NGC 5128 (Centaurus A). Our result shows the source has a strong mekal component. The derived plasma properties from the temperature $kT = 0.68 \pm 0.03$ keV and normalization $K = 4.1 \pm 0.04 \times 10^{-5}$ are $n \geq 7.6 \text{ cm}^{-3}$, $E \leq 5.1 \times 10^{51}$ erg and $t \leq 1.1 \times 10^6$ yr. The X-ray source corresponds to a bright optical source in the DSS image (Kraft et al. 2001). The optical counterpart is included in the USNO-B1.0 catalog (Monet et al. 2003) with the apparent magnitude $m_{B2} = 10.67$ mag and $m_{R2} = 9.44$ mag, corresponding to the absolute magnitude $M_{B2} = -17.8$ mag and $M_{R2} = -19.0$ mag.

No. 26 (NGC 5457) The source is located $6'$ west of the nucleus of NGC 5457 (M101), with a relatively low luminosity ($L < 10^{39}$ erg/s for the best-fitting model) in this *XMM* observation. The mekal component is

prominent in this observation with spectral parameters $kT = 0.67 \pm 0.04$ keV and $K = 1.7 \pm 0.2 \times 10^{-5}$. We derive the plasma parameters $n \geq 4.0 \text{ cm}^{-3}$, $E \leq 7.8 \times 10^{51}$ erg and $t \leq 2.1 \times 10^6$ yr. This source also has an optical counterpart in the DSS image. The optical counterpart is in the GSC catalog (Morrison et al. 2001) and has an apparent magnitude $m_V = 15.5 \pm 0.3$ mag, corresponding to an absolute magnitude $M_V = -13.7$ mag. This source is also observed by the Optical Monitor on-board *XMM* with an absolute magnitude $M_{UVW1} = -10.8$ mag.

One plausible interpretation for the hot diffuse plasma components is that they are young supernova remnants. The derived density, total energy, and cooling time are consistent with this interpretation. The X-ray luminosities and temperatures of these three sources are similar to recent supernovae (e.g. SN 1979C, Immler & Lewin 2003; Immler et al. 2005). The high absolute magnitudes of the optical counterparts indicates they are not normal stars. Comparison with the late-time absolute magnitude of SN 1979C ($M_B = -12.1$ mag, $M_{UVW1} = -13.6$ mag), suggests that they may be supernova remnants which are several tens years old. We do not find supernovae counterparts on the IAU supernova list¹, but the supernova may easily have been missed. Source 22 is found to have noise power above the Poisson level, which could not be produced by a spatially extended source. However, more than 2/3 of the luminosity arises from the power-law emission. The low frequency noise for source 22 (the first two points in Fig. 7) is strongest in the 1–10 keV band, where the energy spectrum is dominated by the power-law component also. Therefore, the variability appears related to the power-law rather than the mekal component and may arise from a central compact object.

5.3. *High temperature sources*

Three sources (3, 6, and 7) have spectra which are strongly curved at high energies in strong contrast to most of the other sources. From the MCD fits, we found that the sources have high temperatures and are either super-Eddington for a stationary black hole or near Eddington for a rapidly rotating black hole. These unusual aspects establish these sources as a distinct class. All three sources have low timing noise with an rms in the 0.001–0.1 Hz band below 0.02.

Foschini et al. (2004) suggested that source 3 (M33 X-8) is a stellar-mass black hole in the high state because its behavior is similar to that of Galactic black hole X-ray binaries. Radio emission with a spectral index similar to microquasars has been found in VLA observations (Gordon et al. 1999), possibly linking this source with microquasars. Foschini et al. (2004) also suggest that the emission may be beamed. Source 7 (in M81, F88 X-6) has also been identified with a weak radio counterpart (Fabbiano 1988; Swartz et al. 2003).

Other interpretations for the high temperatures in some ULXs include intermediate mass black holes in the Kerr metric (Makishima et al. 2000) or black holes of several tens of solar masses with slim accretion disks (advection dominated optically thick disks) emitting at super-Eddington luminosities (Ebisawa et al. 2003). These interpretations are based on results showing that single multicolor disk blackbody spectrum provide the

¹ <http://cfa-www.harvard.edu/iau/lists/Supernovae.html>

best fits for high-temperature ULXs (Makishima et al. 2000). Our results based on the high quality spectra available from *XMM-Newton* show that a single MCD provides a significantly worse fit than a Comptonization model. A MCD model with an additional power-law component can provide an equally good fit, but the power-law is dominant at low energies, which is different from the behavior usually seen from Galactic black hole binaries where the power-law component is usually weak when then source is in the thermal dominant state which shows prominent MCD emission near 1 keV (McClintock & Remillard 2004). In the Comptonization model, a high electron column density $\sim 3 \times 10^{25} \text{ cm}^{-2}$, is required to produce the observed optical depths (Makishima et al. 2000). Since heavy ions would not be ionized at the inferred temperatures, strong Fe-K absorption should be observed unless the material has

very low metallicity. No Fe-K absorption is apparent in the data, but the constraints are weak due to the limited statistics at high energies. Adding a smeared edge model to the Comptonization spectra with a central energy of 7 keV, optical depths up to $\tau \sim 6$ are allowed, depending on the edge width. Lack of Fe-K absorption would argue against accepting the Comptonization model.

We thank the referee for some useful suggestions which improved our paper. We acknowledge partial support from Chandra grants GO4-5086 and GO4-5035. PK thanks the Aspen Center for Physics for its hospitality during the workshop, “Compact Objects in External Galaxies”, and acknowledges partial support from a University of Iowa Faculty Scholar Award.

REFERENCES

- Colbert, E.J.M., & Mushotzky, R.F. 1999, *ApJ*, 519, 89
 Colbert, E.J.M., & Ptak, A.F. 2002, *ApJS*, 143, 25
 Cropper, M. et al. 2004, *MNRAS*, 349, 39
 Dewangan, G.C. et al. 2004, *ApJ*, 608, L57
 Dickey, J.M., & Lockman, F.J. 1990, *ARA&A*, 28, 215
 Ebisawa, K. et al. 2003, *ApJ*, 597, 780
 Fabbiano, G. 1988, *ApJS*, 235, 544
 Fabbiano, G. 1989, *ARA&A*, 27, 87
 Fabbiano, G., & White, N.E. 2003, *Compact Stellar X-ray Sources in Normal Galaxies*, eds. W.H.G. Lewin and M. van der Klis (Cambridge: Cambridge Univ. Press), in press, astro-ph/0307077
 Foschini, L. et al. 2004, *A&A*, 416, 529
 Gilfanov, M. & Arefiev, V. 2005, submitted to *MNRAS*, astro-ph/0501215
 Gordon, S.M. et al. 1999, *ApJS*, 120, 247
 Immler, R. et al. 2005, submitted to *ApJ*, astro-ph/0503678
 Immler, R., & Lewin, W.H.G. 2003, *X-Ray Supernovae*, ed. K.W. Weiler (Springer-Verlag), 91, astro-ph/0202231
 Kaaret, P. et al. 2001, *MNRAS*, 321, L29
 Kaaret, P. et al. 2003, *Science*, 299, 365
 Kaaret, P. et al. 2004, *MNRAS*, 351, L83
 King, A.R. et al. 2001, *ApJ*, 552, L109
 K rding, E. et al. 2002, *A&A*, 382, L13
 Kraft, R.P. et al. 2001, *ApJ*, 560, 675
 Kubota, A. et al. 2001, *ApJ*, 547, L119
 La Parola, V. et al. 2001, *ApJ*, 556, 47
 Lira, P. et al. 2000, *MNRAS*, 319, 17
 Liu, Q.Z., & Mirabel, I.F. 2005, *A&A*, 429, 1125
 Makishima, K. et al. 1986, *ApJ*, 308, 635
 Makishima, K. et al. 2000, *ApJ*, 535, 632
 McClintock, J.E., & Remillard, R.A. 2004, *Black Hole Binaries*, eds. W.H.G. Lewin and M. van der Klis (Cambridge: Cambridge Univ. Press), in press, astro-ph/0306213
 Mewe, R. et al. 1995, *Legacy* 6, 16
 Miller, J.M. et al. 2003, *ApJ*, 585, L37
 Miller, J.M. et al. 2004, *ApJ*, 614, L117
 Miller, M.C. & Colbert, E.J.M. 2004, *Int. J. Mod. Phys.*, 13, 1, astro-ph/0308402
 Mitsuda, K. et al. 1984, *PASJ*, 36, 741
 Monet, D.G. et al. 2003, *AJ*, 125, 984
 Morrison J.E. et al. 2001, *AJ*, 121, 1752
 Pakull, M.W., & Mirioni, L. 2003, in *ESA SP-488, New Visions of the X-ray Universe in the XMM-Newton and Chandra Era*, ed. F. Jansen (Noordwijk: ES-TEC/ESA), in press (astro-ph/0202488)
 Ptak, A., & Griffiths R. 1999, *ApJ*, 517, L85
 Soria, R. et al. 2004, *MNRAS*, 423, 955
 Swartz, D.A. et al. 2003, *ApJS*, 144, 213
 Swartz, D.A. et al. 2004, *ApJS*, 154, 519
 Sunyaev, R.A., & Titarchuk, L.G. 1980, *A&A*, 86, 121
 van der Klis, M. 1988, in *Timing Neutron Stars*, ed. H. Ogelmen & E. P. J. van den Heuvel (Dordrecht: Kluwer), 27
 Wang, Q.D. et al. 2004, *ApJ*, 609, 113

TABLE 1
XMM OBSERVATIONS OF ULXS IN NEARBY GALAXIES

No.	Host Galaxy	RA (J2000)	Dec (J2000)	Dist. (Mpc)	Obs Date	Exposure ^a (ks)	Ref. ^b
1	Circinus	14 12 53.52	-65 22 54.7	4.0	08/06/01	61.1/91.1	1
2	IC 342	03 45 55.7	+68 04 58	3.9	02/11/01	4.9/5.1	2
3	NGC 598	01 33 50.89	+30 39 37.2	0.9	08/04/00	6.5/11.9	1
4	NGC 1313	03 18 19.9	-66 29 07	3.7	10/17/00	17.4/28.0	2
5	NGC 1313	03 18 22.2	-66 36 01	3.7	10/17/00	17.4/28.0	2
6	NGC 2403	07 36 25.55	+65 35 40.0	3.1	09/12/04	50.6/69.1	1
7	NGC 3031	09 55 32.98	+69 00 33.4	3.6	04/22/01	87.8/125.4	1
8	NGC 3031	09 57 54.4	+69 03 43	3.6	04/16/02	7.7/7.7	2
9	NGC 3628	11 20 15.76	+13 35 13.7	10.0	11/27/00	37.7/41.2	1
10	NGC 4258	12 18 43.86	+47 17 31.5	7.7	12/08/00	12.2/14.4	1
11	NGC 4258	12 18 57.84	+47 16 07.1	7.7	12/08/00	12.2/14.4	1
12	NGC 4395	12 26 01.8	+33 31 34	3.6	11/30/03	86.9/96.1	2
13	NGC 4449	12 28 17.83	+44 06 33.9	3.7	06/02/02	10.6/11.8	1
14	NGC 4485	12 30 30.56	+41 41 42.3	7.8	05/27/02	11.5/12.0	1
15	NGC 4490	12 30 36.32	+41 38 37.8	7.8	05/27/02	11.5/12.0	1
16	NGC 4490	12 30 43.25	+41 38 18.4	7.8	05/27/02	11.5/12.0	1
17	NGC 4559	12 35 51.71	+27 56 04.1	10.3	05/27/03	33.7/36.4	1
18	NGC 4559	12 35 58.57	+27 57 41.8	10.3	05/27/03	33.7/36.4	1
19	NGC 4631	12 41 55.56	+32 32 16.9	7.6	06/28/02	44.9/53.2	1
20	NGC 4945	13 05 21.94	-49 28 26.6	3.7	01/21/01	17.9/17.9	1
21	NGC 4945	13 05 32.89	-49 27 34.1	3.7	01/21/01	17.9/17.9	2
22	NGC 5128	13 25 07.4	-43 04 06	4.9	02/02/01	16.8/16.8	2
23	NGC 5204	13 29 38.61	+58 25 05.6	4.5	01/06/03	15.4/15.4	1
24	NGC 5236	13 37 20.1	-29 53 46	4.7	01/27/03	18.9/24.1	2
25	NGC 5408	14 03 19.61	-41 22 59.6	4.8	01/28/03	2.7/4.0	3
26	NGC 5457	14 02 29.89	+54 21 19.0	7.0	06/04/02	21.6/36.5	1
27	NGC 5457	14 04 14.28	+54 26 03.6	7.0	06/04/02	21.6/36.5	1
28	UGC 4305	08 19 28.99	+70 42 19.4	3.4	04/10/02	4.7/4.7	1

^aThe clean/total exposure of pn CCDs, or mos CCDs in case pn data are not used.

^bThe catalog from which the coordinates of the ULXs and the distance of the host galaxy are taken; (1)–Swartz et al. (2004), (2)–Colbert & Ptak (2002), (3)–Liu & Mirabel (2005).

TABLE 2
 SPECTRAL PARAMETERS AND VARIABILITIES OF SELECTED ULXs.

No.	Model	n'_H ^a (10^{21} cm ⁻²)	n_H (10^{21} cm ⁻²)	Γ/τ ^b	kT ^c (keV)	L ^d (10^{40} erg/s)	χ^2/dof	rms ^e (0.001–0.1 Hz)
1	powerlaw	5.33	$10.9^{+0.7}_{-0.7}$	$3.30^{+0.12}_{-0.12}$...	$0.42^{+0.01}_{-0.14}$	340.4/265	< 0.131
	diskbb		$5.6^{+0.4}_{-0.4}$...	$0.74^{+0.03}_{-0.03}$	$0.0764^{+0.0002}_{-0.0067}$	267.4/265	
2	powerlaw	3.03	$5.8^{+0.6}_{-0.6}$	$1.67^{+0.09}_{-0.05}$...	$0.44^{+0.04}_{-0.05}$	142.9/153	< 0.069
	diskbb		$3.1^{+0.1}_{-0.1}$...	$2.01^{+0.17}_{-0.15}$	$0.48^{+0.01}_{-0.04}$	169.2/153	
3	diskbb	0.56	$0.56^{+0.02}_{+0.00}$...	$1.12^{+0.01}_{-0.02}$	$0.156^{+0.001}_{-0.003}$	909.0/692	< 0.003
	powerlaw+diskbb		$1.7^{+0.2}_{-0.2}$	$2.34^{+0.16}_{-0.13}$	$1.14^{+0.06}_{-0.06}$	$0.226^{+0.006}_{-0.003}$	694.1/690	
	compst		$1.6^{+0.1}_{-0.1}$	$20.5^{+0.9}_{-0.8}$	$1.18^{+0.05}_{-0.05}$	$0.220^{+0.003}_{-0.003}$	700.1/691	
4	powerlaw	0.39	$1.9^{+0.1}_{-0.1}$	$1.95^{+0.04}_{-0.04}$...	$0.59^{+0.02}_{-0.01}$	766.2/627	0.028 ± 0.013
	powerlaw+diskbb		$3.0^{+0.4}_{-0.3}$	$1.74^{+0.06}_{-0.06}$	$0.20^{+0.02}_{-0.02}$	$0.81^{+0.03}_{-0.06}$	598.9/625	
5	powerlaw	0.39	$2.7^{+0.2}_{-0.2}$	$2.45^{+0.08}_{-0.08}$...	$0.29^{+0.01}_{-0.01}$	266.9/252	< 0.077
	powerlaw+diskbb		$2.9^{+0.7}_{-0.3}$	$2.19^{+0.18}_{-0.15}$	$0.23^{+0.05}_{-0.06}$	$0.30^{+0.02}_{-0.05}$	244.8/250	
6	diskbb	0.41	$1.6^{+0.1}_{-0.1}$...	$1.04^{+0.02}_{-0.02}$	$0.170^{+0.001}_{-0.003}$	1019.2/869	< 0.012
	powerlaw+diskbb		$4.4^{+1.0}_{-0.7}$	$3.5^{+0.7}_{-0.5}$	$1.16^{+0.04}_{-0.04}$	$0.42^{+0.01}_{-0.04}$	952.3/867	
	compst		$3.0^{+0.1}_{-0.2}$	$21.5^{+1.3}_{-1.1}$	$1.04^{+0.05}_{-0.05}$	$0.232^{+0.007}_{-0.005}$	942.6/868	
7	diskbb	0.42	$1.3^{+0.1}_{-0.1}$...	$1.29^{+0.03}_{-0.03}$	$0.43^{+0.01}_{-0.01}$	399.9/310	< 0.008
	powerlaw+diskbb		$4.0^{+1.4}_{-0.7}$	$3.2^{+1.0}_{-0.5}$	$1.51^{+0.06}_{-0.08}$	$0.87^{+0.02}_{-0.07}$	317.7/308	
	compst		$2.7^{+0.1}_{-0.2}$	$20.3^{+1.2}_{-1.3}$	$1.31^{+0.08}_{-0.07}$	$0.56^{+0.02}_{-0.02}$	315.8/309	
8	powerlaw	0.42	$2.0^{+0.1}_{-0.1}$	$1.88^{+0.03}_{-0.03}$...	$1.69^{+0.03}_{-0.03}$	979.3/944	< 0.010
	powerlaw+diskbb		$2.4^{+0.2}_{-0.2}$	$1.81^{+0.04}_{-0.05}$	$0.22^{+0.05}_{-0.03}$	$1.85^{+0.05}_{-0.11}$	942.0/942	
9	powerlaw	0.22	$6.6^{+0.5}_{-0.4}$	$1.65^{+0.07}_{-0.06}$...	$1.06^{+0.05}_{-0.05}$	296.5/280	< 0.061
10	powerlaw	0.12	$1.3^{+0.5}_{-0.4}$	$1.8^{+0.2}_{-0.2}$...	$0.13^{+0.02}_{-0.01}$	43.8/40	< 0.498
11	powerlaw	0.12	$2.6^{+0.7}_{-0.5}$	$2.00^{+0.10}_{-0.17}$...	$0.16^{+0.02}_{-0.02}$	48.1/46	< 0.253
	diskbb		$0.7^{+0.4}_{-0.3}$...	$1.20^{+0.19}_{-0.16}$	$0.10^{+0.01}_{-0.02}$	55.8/46	
12	powerlaw+mekal	0.14	$1.6^{+0.1}_{-0.1}$	$3.73^{+0.11}_{-0.10}$	$0.78^{+0.01}_{-0.04}$	$0.20^{+0.01}_{-0.01}$	292.6/217	< 0.045
	powerlaw+diskbb		$1.1^{+0.3}_{-0.2}$	$3.1^{+0.3}_{-0.2}$	$0.25^{+0.01}_{-0.02}$	$0.120^{+0.022}_{-0.002}$	375.7/217	
13	powerlaw	0.14	$6.5^{+1.0}_{-0.9}$	$2.25^{+0.16}_{-0.08}$...	$0.19^{+0.01}_{-0.03}$	80.9/90	< 0.073
	diskbb		$2.7^{+0.6}_{-0.6}$...	$1.26^{+0.12}_{-0.11}$	$0.096^{+0.001}_{-0.014}$	112.4/90	
14	powerlaw	0.18	$2.6^{+0.5}_{-0.5}$	$2.06^{+0.17}_{-0.15}$...	$0.50^{+0.05}_{-0.04}$	64.3/57	< 0.092
	diskbb		$0.8^{+0.3}_{-0.3}$...	$1.12^{+0.12}_{-0.11}$	$0.29^{+0.01}_{-0.04}$	74.5/57	
15	powerlaw	0.18	$3.2^{+0.3}_{-0.3}$	$2.08^{+0.09}_{-0.09}$...	$0.63^{+0.04}_{-0.04}$	145.4/142	< 0.077
	diskbb		$1.1^{+0.2}_{-0.2}$...	$1.25^{+0.08}_{-0.07}$	$0.38^{+0.01}_{-0.03}$	159.6/142	
16	powerlaw	0.18	$6.8^{+0.9}_{-0.8}$	$2.59^{+0.16}_{-0.15}$...	$0.79^{+0.04}_{-0.17}$	97.2/89	< 0.132
	diskbb		$3.3^{+0.5}_{-0.5}$...	$0.98^{+0.07}_{-0.07}$	$0.31^{+0.01}_{-0.04}$	94.8/89	
17	powerlaw	0.15	$1.3^{+0.1}_{-0.1}$	$2.39^{+0.06}_{-0.05}$...	$1.55^{+0.06}_{-0.04}$	442.2/360	< 0.038
	powerlaw+diskbb		$1.8^{+0.4}_{-0.2}$	$2.13^{+0.09}_{-0.07}$	$0.17^{+0.01}_{-0.03}$	$1.94^{+0.11}_{-0.13}$	353.0/358	
18	powerlaw	0.15	$1.2^{+0.1}_{-0.1}$	$1.97^{+0.06}_{-0.05}$...	$1.30^{+0.06}_{-0.05}$	238.6/256	< 0.061
19	powerlaw	0.13	$2.7^{+0.3}_{-0.3}$	$2.07^{+0.10}_{-0.10}$...	$0.51^{+0.03}_{-0.03}$	127.1/128	< 0.049
	diskbb		$0.7^{+0.2}_{-0.2}$...	$1.20^{+0.08}_{-0.08}$	$0.30^{+0.01}_{-0.02}$	159.3/128	
20	powerlaw	1.55	$5.3^{+0.9}_{-0.8}$	$2.5^{+0.2}_{-0.2}$...	$0.08^{+0.01}_{-0.02}$	73.8/59	< 0.160
	diskbb		$2.7^{+0.6}_{-0.5}$...	$0.85^{+0.09}_{-0.08}$	$0.033^{+0.001}_{-0.006}$	67.1/59	
21	powerlaw	1.54	$5.1^{+0.7}_{-0.6}$	$1.76^{+0.10}_{-0.09}$...	$0.13^{+0.01}_{-0.01}$	167.0/155	< 0.073
	diskbb		$2.7^{+0.4}_{-0.4}$...	$1.69^{+0.13}_{-0.12}$	$0.09^{+0.01}_{-0.01}$	151.3/155	
22	powerlaw+mekal	0.87	$0.87^{+0.19}_{+1.00}$	$3.01^{+0.19}_{-0.11}$	$0.68^{+0.03}_{-0.03}$	$0.066^{+0.004}_{-0.008}$	179.0/147	< 0.069
	powerlaw+diskbb		$1.1^{+0.2}_{-0.2}$	$2.1^{+1.6}_{-1.3}$	$0.26^{+0.01}_{-0.06}$	$0.11^{+0.54}_{-0.01}$	266.1/147	
23	powerlaw	0.14	$0.6^{+0.1}_{-0.1}$	$2.05^{+0.04}_{-0.04}$...	$0.46^{+0.01}_{-0.01}$	606.2/574	0.011 ± 0.005
	powerlaw+diskbb		$0.4^{+0.1}_{-0.1}$	$1.77^{+0.09}_{-0.10}$	$0.31^{+0.04}_{-0.04}$	$0.45^{+0.05}_{-0.02}$	571.1/572	
24	powerlaw	0.37	$1.5^{+0.2}_{-0.2}$	$2.45^{+0.10}_{-0.10}$...	$0.17^{+0.01}_{-0.01}$	267.5/236	< 0.045
25	powerlaw	0.56	$1.4^{+0.2}_{-0.2}$	$3.06^{+0.14}_{-0.12}$...	$0.90^{+0.04}_{-0.04}$	218.4/171	0.100 ± 0.010
	powerlaw+diskbb		$1.1^{+0.2}_{-0.2}$	$2.3^{+0.3}_{-0.2}$	$0.21^{+0.03}_{-0.03}$	$0.73^{+0.10}_{-0.06}$	177.9/169	
26	powerlaw+mekal	0.11	$0.4^{+0.2}_{-0.2}$	$2.6^{+0.3}_{-0.1}$	$0.67^{+0.04}_{-0.04}$	$0.08^{+0.01}_{-0.01}$	115.5/86	< 0.465
	powerlaw+diskbb		$1.4^{+0.9}_{-0.9}$	$1.3^{+0.8}_{-1.4}$	$0.23^{+0.03}_{-0.04}$	$0.181^{+0.005}_{-0.077}$	160.7/86	
27	powerlaw	0.12	$1.6^{+0.3}_{-0.3}$	$2.8^{+0.2}_{-0.2}$...	$0.28^{+0.02}_{-0.02}$	101.0/77	< 0.336
28	powerlaw	0.34	$1.8^{+0.1}_{-0.1}$	$2.73^{+0.04}_{-0.03}$...	$1.85^{+0.03}_{-0.03}$	892.8/731	< 0.004
	powerlaw+diskbb		$1.5^{+0.2}_{-0.2}$	$2.45^{+0.11}_{-0.11}$	$0.31^{+0.04}_{-0.04}$	$1.52^{+0.11}_{-0.03}$	864.6/729	

^aAbsorption column density of the Milky Way (Dickey & Lockman 1990)

^b Γ means the photon index for models including a power-law component; τ means the optical depth for the compst model.

^c kT stands for the inner disk temperature for the diskbb model, the plasma temperature for the mekal model, and the electron temperature for the compst model.

^dUnabsorbed X-ray luminosity in the energy range 0.3–10 keV.

^erms variabilities in the frequency range 0.001–0.1 Hz. The rms values are not associated with the spectral models, while in Fig. 6 the luminosity is selected from the best-fitted model.